INTERNATIONAL JOURNAL OF HYDROGEN ENERGY XXX (2016) 1–10

Available online at www.sciencedirect.com

ScienceDirect

journal homepage: www.elsevier.com/locate/he

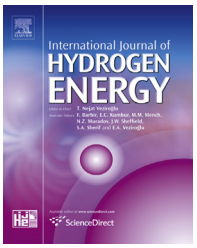

Simple fabrication of porous NiO nanoflowers: Growth mechanism, shape evolution and their application into Li-ion batteries

Y. Bahari Mollamahale [a], Zong Liu [b], Yongda Zhen [c], Zhi Qun Tian [b,*], D. Hosseini [d], Luwei Chen [e], Pei Kang Shen [b]

[a] Nanotechnology Department, University of Guilan, Rasht, Guilan, Iran
[b] Collaborative Innovation Center of Renewal Energy Materials, Guangxi University, Nanning, China
[c] Singapore Polytechnic, 500 Dover Road, Singapore
[d] Institute for Energy Technology, ETH Zurich, Switzerland
[e] Institute of Chemical and Engineering Sciences, A*STAR (Agency for Science, Technology and Research), 1Pesek Road, Jurong Island, Singapore

ARTICLE INFO

Article history:
Received 16 April 2016
Received in revised form
20 May 2016
Accepted 21 May 2016
Available online xxx

Keywords:
NiO
Nanoflowers
Shape evolution
Lithium-ion batteries
Electrochemical properties

ABSTRACT

Tailoring the shape of nanomaterials is a key factor to control their properties. In this presentation, individual porous NiO nanoflowers via α-$Ni(OH)_2$ were fabricated through a simple solvothermal process without any surfactants or growth templates and their application in lithium battery was investigated. In the method, nickel acetate and urea were used as starting materials in ethanol media at 190 °C for 3 h followed by calcination at 400 °C. Electron microscopy studies revealed that initially fine nanoparticles precipitate during solvothermal treatment which then undergo aggregation and self-assembly resulting in nanoflowers. In prolonged time, each nanoflower gives rise to a solid well-faceted microparticle. The electrochemical performance of the NiO nanoflowers was investigated by cyclic voltammetry and conventional galvanostatic charge–discharge tests. The results showed an initial high discharge capacity of ~1330 $mAhg^{-1}$ after 10 cycles at 0.1 C rate and a stable capacity of 630 $mAhg^{-1}$ after 40 cycles in the range of 0.01–3.0 V with the excellent columbic efficiency of ~94%, suggesting that they have a very promising potential in the future application for lithium ion battery.

Introduction

Lithium ion battery, a highly efficient energy storage device, has been widely applied to various kinds of portable electronics and is becoming the dominant power source for electric vehicles [1,2]. In order to improve the intercalation and deintercalation rate of lithium ions in electrode materials, capacity, cyclability and safety of lithium ion battery, nano-sized electrode materials have attracted considerable attentions over the past few years leading to fabrication of new nanostructured materials with superior

* *Corresponding author*. Tel.: +86 7113237330.
E-mail address: tianzhiqun@gxu.edu.cn (Z.Q. Tian).

http://dx.doi.org/10.1016/j.ijhydene.2016.05.193

properties in Li-ion batteries technology. Specially, many efforts have been performed for fabrication of three dimensional (3D) hierarchal nanostructures constructed by self-assembly of low dimensional building blocks such as nanowires [3–6], nanotubes [7–9], nanoflakes [10–12], nanoflowers [13–16] due to that the nanostructure materials can improve the performance of batteries in principle [17–19]. It is believable that the overall activity of a battery depends on not only the intrinsic properties of active materials but also their crystallite size and shape. Therefore, tailoring the morphology and the dimension of the active battery material can manipulate its electrochemical behavior.

Metal oxide nanostructures such as NiO, CoO, Fe_3O_4 and CuO are promising anode materials in Li-ion batteries [16,20]. Specifically, there have been lots of interests on using NiO nanostructures due to their high theoretical capacity, low cost, low toxicity, high chemical/thermal stability and widespread availability [21,22]. To date, various NiO nanostructures with different morphologies such as nanoparticles [23], nanowires [24], nanoplatelets [25], nanowalls [26], nanoflakes [2], nanotubes [27], and nanoflowers [28] have been reported. Among them, NiO nanoflowers have been considered by researchers as an effective architecture in improving the electrochemical properties due to the ease of accessibility for the electrolyte, large surface-to-volume ratio and short diffusion length for lithium intercalation [29,30]. So far, the reported synthesis methods for NiO nanoflowers mostly include a complexing agent such as ammonium hydroxide and dimethylglyoxime, a surfactant such as polyethyleneglycol (PEG), ploy vinylparrolidone (PVP), cetyltrimethyl ammonium bromide (CTAB) or sodium dodecyl sulfate (SDS) and employing high temperatures, a lamp or microwave [28,31–34]. Moreover, the primary structure is β-$Ni(OH)_2$ or another intermediate structure and preserving the structure after calcination is quite important to get to NiO nanoflowers. For example Zhu et al. synthesized 3D flower-like $Ni(OH)_2$ architectures using nickel nitrate as precursor and PEG as surfactant in ethanol media together with dropwise adding of NH_3 as complexing agent and then employing a high temperature of 160 °C in microwave [32]. Some efforts have been done for surfactant-free synthesis of $Ni(OH)_2$ as well. For instance, Yang et al. [34] developed a flower-like $Ni_3(NO3)_2(OH)_4$ using nickel nitrate as precursor and pure ethanol as solvent at 120 °C which after calcination resulted in NiO. However, the flower-like structure was seriously damaged after calcination. β-$Ni(OH)_2$ nanoflowers has been also reported thorough aqueous solution of nickel chloride and urea and using NH_3 as complexing agent at 120 °C but keeping the morphology safe after calcination [28].

In this paper, we report a facile and surfactant-free method for fabrication of 3D flower-like α-$Ni(OH)_2$ nanostructure which converts to NiO after calcination with preserving the morphology. Growth mechanisms, morphological and structural evolutions have also been discussed in detail which could be helpful for further investigations and tailoring the desired architectures in the future. The electrochemical performance of the prepared NiO nanoflowers in Li-ion battery was also investigated.

Experimental

Chemicals

All the chemicals were analytical grade reagents purchased from Sigma–Aldrich except 1-Hexanol which was prepared from Fischer. The chemicals used as received without any further purifications. Doubly distilled water was used during all the experiments.

Preparation of NiO nanoflowers

In a typical synthesis, 0.5 g of nickel acetate tetrahydrate ($Ni(ac)_2.4H_2O$) and 0.25 g of urea were dissolved in 30 mL ethanol and stirred magnetically until a homogenous solution was obtained. The homogenous solution was then transferred to a Teflon-lined stainless steel autoclave with a total volume of 45 mL. The sealed autoclave was then placed in an oven at 190 °C for different times ranging from 3 h to 24 h. After cooling down to room temperature naturally in air, the precipitate was filtered, washed with ethanol and deionized water for several times to remove the impurities and dried in oven at 60 °C for 24 h. The dried green powder was finally calcined at a muffle furnace through heating with a ramp rate of 10 °C/min from room temperature to 400 °C and then leveled off at this temperature for additional 1 h followed by cooling down to room temperature. The black NiO powder was then collected for characterization and further experiments. Similar experiments were conducted to understand the key factors affecting the formation of nanoflowers. Table 1 lists details for each experiment. The related samples were labeled as S1 (with different reaction times) to S5.

Characterization

Powder X-ray diffraction (XRD) patterns were collected with a Bruker D8 X-ray diffraction system equipped with Cu K_αr-adiation ($k_\alpha = 0.154$ nm). The profiles were collected at a step width of 0.02° in the 2θ range from 20° to 90°. Scanning electron microscope (SEM) images were obtained with a field-emission scanning electron microscope (FESEM, JEOL JSM-6700F). For imaging by Transmission electron microscopy (TEM) using a FEI TecnaiG^2 microscope, small amount of the sample was dispersed in ethanol and two drops were poured on a copper grid followed by drying in an oven at 60 °C for 4 h. NiO nanoflowers surface area was determined by Brunauer–Emmett–Teller (BET) experiment and a ASAP2020 volumetric adsorption analyzer (Micromeritics, USA) was employed by measuring the adsorption of N_2.

Electrochemical properties were measured on electrodes prepared by compressing a mixture of as-synthesized powders, carbon black, and poly (vinyl difluoride) (PVDF) binder in a weight ratio of 70:15:15 and pasting the mixture on copper foil, following by being dried at 110 °C for 10 h. The foil was cut into circular strips of 12 mm in diameter to serve as the working electrodes. The mass loading of active materials was 1.8 mg/cm^2. Pure lithium foil was used for the counter and reference electrodes. The electrolyte was composed of a 1 M $LiPF_6$ dissolved in ethylene carbonate/dimethyl carbonate/

Please cite this article in press as: Mollamahale YB, et al., Simple fabrication of porous NiO nanoflowers: Growth mechanism, shape evolution and their application into Li-ion batteries, International Journal of Hydrogen Energy (2016), http://dx.doi.org/10.1016/j.ijhydene.2016.05.193

Table 1 – Materials used in each experiment (T = 190 °C for all the samples).

Sample	Nickel precursor	Media	Additives	Time
S1	$Ni(ac)_2.4H_2O$(0.5 g)	Ethanol (30 cc)	Urea (0.25 g)	0
S1-2.5h				2.5 h
S1-3h				3 h
S1-4h				4 h
S1-4.5h				4.5 h
S1-8h				8 h
S1-24h				24 h
S2	$Ni(ac)_2.4H_2O$(0.5 g)	1-Hexanol (30 cc)	Urea (0.25 g)	3 h
S3	$Ni(ac)_2.4H_2O$(0.5 g)	Ethanol (25 cc) $+H_2O$(5 cc)	Urea (0.25 g)	3 h
S4	$Ni(ac\ ac)_2$ (0.5 g)	Ethanol (30 cc)	Urea (0.25 g)	3 h
S5	$Ni(ac)_2.4H_2O$(0.5 g)	Ethanol (30 cc)	None	3 h

diethyl carbonate (EC/DMC/DEC) with the weight ratio of 1:1:1. Celgard 2400 was used as the separator film to isolate the two electrodes. The cell was assembled in an argon-filled glove box where moisture and oxygen concentrations were strictly limited to below 1 ppm. Capacity and Rate capability tests of the electrodes were then carried out systematically using a LAND-CT2001A instrument in a potential range of 0.01–3.0 V. Cyclic voltammetry was performed on a Solartron 1260/1287 electrochemical work station.

Results and discussion

Structure and morphology of the prepared samples

The crystal structure and phase transformation of the samples were studied by XRD. The XRD patterns for the sample S1-3h before and after calcination are represented in Fig. 1a and b, respectively. The peaks in Fig. 1a match with α-$Ni(OH)_2$ crystallized in F.C.C. structure according to JCPDS card no. 38-0715. The peaks, however, are very broad indicating the low crystallinity of α-$Ni(OH)_2$. After calcination of α-$Ni(OH)_2$ at 400 °C for 1 h, the green color turned black and the structure was totally converted to well-crystallized NiO with a F.C.C. structure (JCPDS card no. 44-159). No evidence of α-$Ni(OH)_2$ was found in the XRD pattern describing the whole phase transformation of the structure to NiO. By Applying Scherrer equation $D = k\lambda/(\beta\cos\theta)$ (1), where D is the main crystallite size, λ is the wavelength of the X-ray radiation (1.54 Å), k is a constant to be taken as 0.9, β is the full width at half maximum height of the peak (FWHM) and θ is the diffraction angle, the crystallite sizes were calculated to be 3 nm and 6 nm for α-$Ni(OH)_2$ and NiO, respectively.

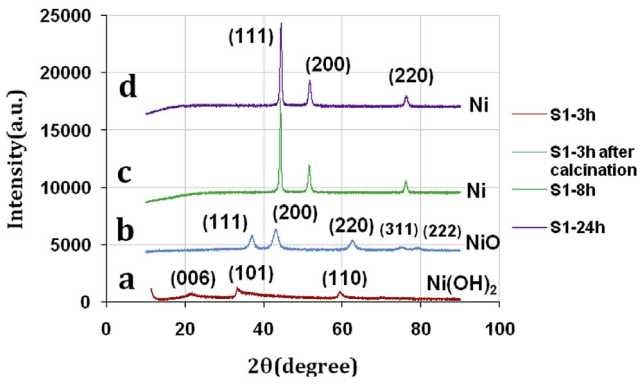

Fig. 1 – XRD patterns for (a) S1-3h before calcination (b) S1-3h after calcination at 400 °C for 1h (c) S1-8h and (d) S1-24h.

Fig. 1c and d demonstrate XRD patterns for the S1 sample with extending the reaction time to 8 h and 24 h (labeled as S1-8h and S1-24h), respectively. The peaks at 44.5°, 51.9° and 76.3° could be indexed to (111), (200), (220) crystal planes of metallic Ni with a F.C.C. unit cell (a = 3.523 Å) based on JSPDS card no. 04-0580, indicating that the α-$Ni(OH)_2$ structure has been totally converted to metallic nickel with the further reaction times. The peaks are sharp suggesting the structures are well crystallized. Applying the Scherrer formula results in 20 nm and 17 nm crystallite size for samples of S1-8 h and S1-24 h, respectively.

Fig. 2 displays SEM and TEM images for the S1 sample before and after calcination.

Fig. 2a shows the morphology of the prepared α-$Ni(OH)_2$ which clearly depicts individual hierarchical nanoflowers have been prepared in large scale. The structure is porous and diameter of each nanoflower constructed of thin petals is about 1 μm. The nanoflowers are homogenous without any further growing structure.

The morphology was preserved after calcination of α-$Ni(OH)_2$ at 400 °C and no major damage was observed resulting in NiO nanoflowers (Fig. 2b).

The thickness of each petal is less than 30 nm from Fig. 2b. TEM observation in Fig. 2c suggests that the ultrathin petals are the building blocks at each nanoflower connected through the bottom to each other resulting in a rose like flower. It seems that each individual petal forms a continuous structure curled around a hole in the middle thus creating a porous structure. For a better understanding we took a higher resolution TEM image from a petal in nanoflower (Fig. 2d). It is interesting that unlike our expectation, each petal in the flower is not a monolithic structure but consists of very fine nanoparticles which aggregated to each other. Therefore, the initial building blocks for nanoflower are tiny nanoparticles with a size less than 5 nm which is in agreement with the particles size obtained from XRD analysis.

The porous nature of the prepared NiO nanoflowers was furthered confirmed by N_2 adsorption–desorption isotherms.

Please cite this article in press as: Mollamahale YB, et al., Simple fabrication of porous NiO nanoflowers: Growth mechanism, shape evolution and their application into Li-ion batteries, International Journal of Hydrogen Energy (2016), http://dx.doi.org/10.1016/j.ijhydene.2016.05.193

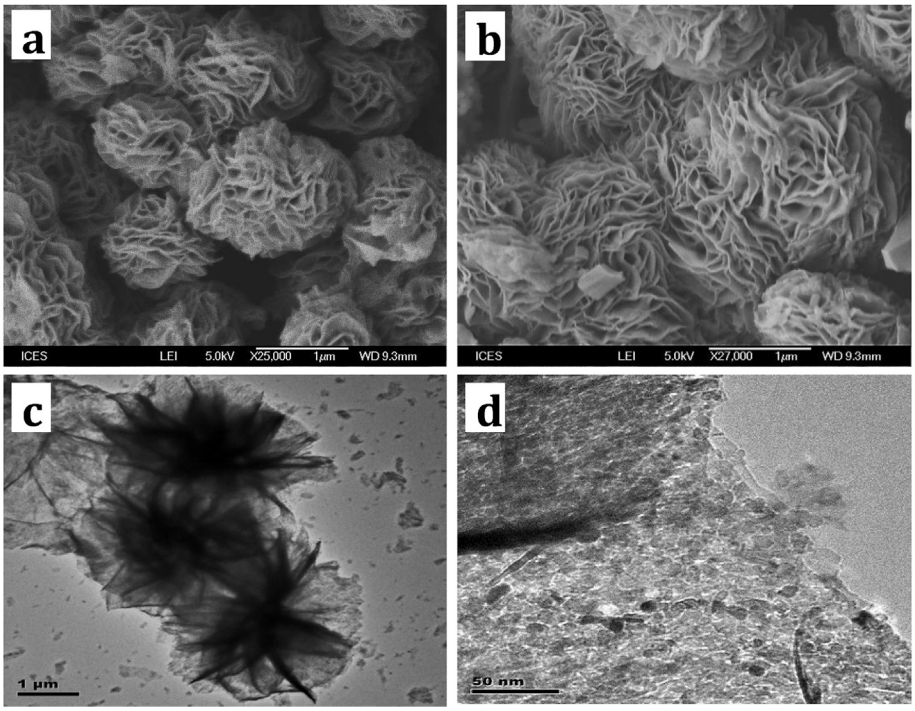

Fig. 2 – SEM images of NiO nanoflowers (a) before and (b) after calcination; (c) and (d) TEM images of NiO nanoflowers at different magnifications.

The isotherms in Fig. 3 are characterized as type IV and show a hysteresis loop which is the characteristic of mesoporous materials. The BET surface area plot (inset of Fig. 3) also delivered a high surface area of 46 $m^2\ g^{-1}$ for the structure.

When the reaction time was further increased to 8 h, nanoflowers were transformed from flower-like structure with ultrathin petals to solid and bulky microparticles (Fig. 4a). As noted before, the structure was also converted from α-$Ni(OH)_2$ to metallic Ni according to the data from XRD (Fig. 1c). Therefore, simultaneously structural and morphological conversions have been occurred. Looking more accurately, these structures are not quite spherical but rather faceted. Therefore, each α-$Ni(OH)_2$ nanoflower gives rise to a faceted solid microparticle but with metallic Ni structure. This may be referred to oxidation of ethanol to aldehyde which is well-known:

$$Ni(OH)_2 + CH_3CH_2OH = Ni + CH_3CHO + 2H_2O \quad (2)$$

Prolonging the reaction time to 24 h, the solid microspheres would be still the dominant structure but it gives rise to more faceted structures (Fig. 4c). TEM images (Fig. 4b and d) are also in agreement with the above discussions, confirming that the Ni microparticles are more uniform in 24 h of reaction time. Polyhedron of Ni microparticles is formed due to Ostwald ripening which results in more uniform and more faceted structures. However, the composition is still Ni suggesting that there would be no more chemical reaction and Ni would be the stable material for the rest of reaction times.

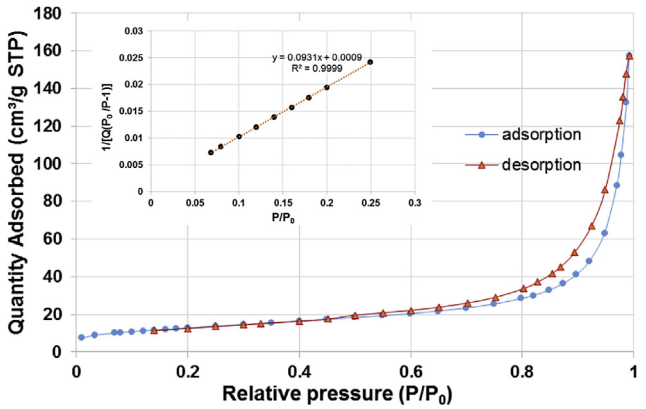

Fig. 3 – Nitrogen adsorption-desorption isotherm of NiO nanoflowers. The inset shows BET surface area plot.

Growth and evolution mechanisms of nanoflowers

The growth mechanism of nanoflower structure is still under further investigations in the community. To date, various types of nanoflowers for NiO and $Ni(OH)_2$ have been described by researchers via very different synthesis method. This is mainly because the formation mechanism of nanoflower structure is complicated and greatly depends on various parameters such as time, temperature, hydrophobic–hydrophilic interactions, hydrogen bonding, electrostatic and van der Walls forces, crystal-face attraction, dipolar fields, and Ostwald ripening [31].

In order to understand the growth conditions for the prepared NiO nanoflowers, several experiments were conducted as listed in Table 1.

Please cite this article in press as: Mollamahale YB, et al., Simple fabrication of porous NiO nanoflowers: Growth mechanism, shape evolution and their application into Li-ion batteries, International Journal of Hydrogen Energy (2016), http://dx.doi.org/10.1016/j.ijhydene.2016.05.193

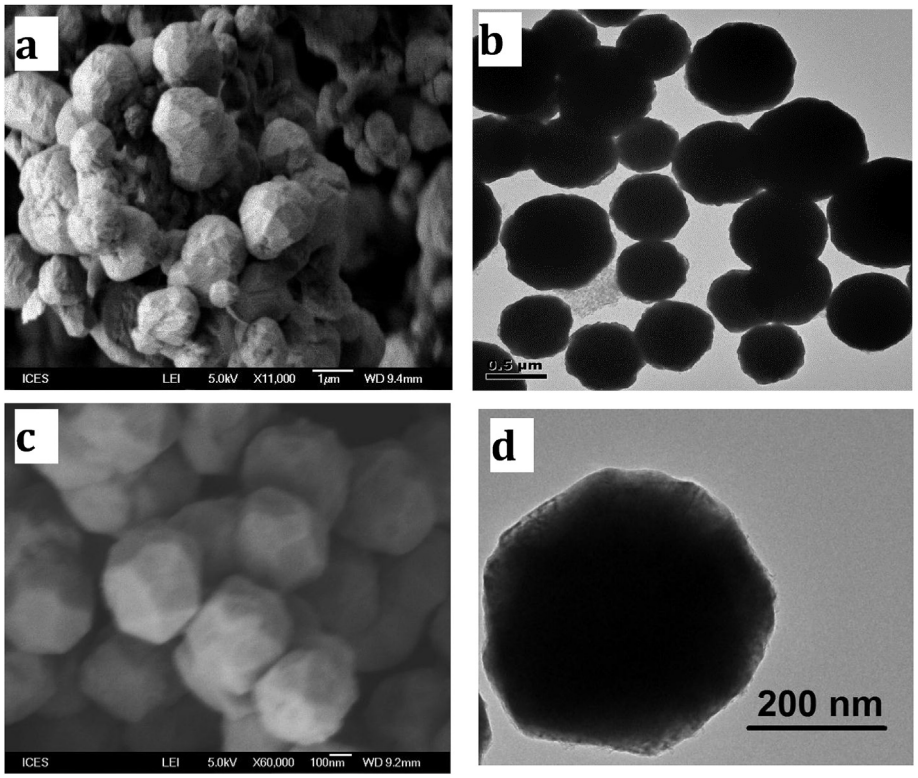

Fig. 4 – SEM and TEM images for (a,b) S1-8h and (c,d) S1-24h, respectively.

As described earlier, each nanoflower initially constructed from fine aggregated nanoparticles (Fig. 2d) which is consistent with the previous works in fabrication of crystals with hierarchical structures and complex morphologies [19,28,35].

The hotspots in the solution are the driving force for nucleation of the initial nanoparticles [31]. Hot spots are mainly originated from heating of the solution creating potentially reaction points in the solution. In the absence of these driving forces no reaction occurs. In all the experiments, the temperature was increased to 190 °C for this aim. It is worth noting that this initially results in supersaturation of nickel precursor as well.

On the other hand, surfactants and organic compounds present in the solution could create hotspots as well [31,36,37]. This was further confirmed when urea was removed from the reaction (S5) in which the amount of collected precipitate was dramatically decreased and nanoflowers morphology was not obtained. It is then concluded that urea favors the nucleation of nanoparticles and their subsequent growth to nanoflowers.

The surface energy of initial crystalline nanoparticles is high which makes them tend to aggregate to minimize the surface energy. Under homogeneous and slow precipitation conditions, aggregated nanoparticles are oriented along a crystal plane which after assembly results in a petal morphology. Fig. 5a surprisingly shows an incomplete nanoflower formed after 2.5 h of reaction treatment (S1-2.5h), confirming the above discussion. The petals then undergo random self-assembly and Ostwald ripening processes giving rise to a flowerlike morphology.

The morphologies of $Ni(OH)_2$ in the presence of two different solvents, 1-Hexanol and a mixture of ethanol and water (5:1 v/v), are demonstrated in Fig. 5 b and c, respectively. Fig. 5b shows the SEM image of $Ni(OH)_2$ in which ethanol was totally replaced by 1-Hexanol resulting in a totally irregular shape. In contrast, when small amount of water was added to ethanol, $Ni(OH)_2$ nanoflakes were surprisingly fabricated (Fig. 5c). The presence of water favors the basic conditions by hydrolysis of CH_3COO ions which promotes the planar growth of crystals [38].

Moreover, this gives the opportunity to hydrolysis of urea as follow:

$$(NH_2)_2CO + H_2O = 2NH_3 + CO_2 \quad (3)$$

$$NH_3 + H_2O = NH_4^+ + OH^- \quad (4)$$

resulting in generation of hydroxyl anions which again favors the formation of nickel hydroxide. Different properties of the solvents such as viscosity, boiling point, polarity, etc. are directly responsible for the nucleation and growth of the particles and therefore different final morphologies [38]. Therefore, ethanol plays a key role in providing the suitable environment for nucleation and growth of the nanoflowers. As reported, solvents, inorganic additives and surfactants could adsorb to certain crystallographic planes and modify the surface energies resulting in a flowerlike morphology [31].

It is worth noting that when $Ni(ac)_2.4H_2O$ was replaced by Ni(ac ac)$_2$, agglomerated nanoparticles were formed (Fig. 5d) suggesting that the nickel source is also a determining factor on the final morphology.

Prolonging the reaction time of S1 to 4 h results in dissolution and recrystallization of the nanoparticles in nanoflowers (S1-4h). Fig. 6a shows a very interesting TEM image in

Please cite this article in press as: Mollamahale YB, et al., Simple fabrication of porous NiO nanoflowers: Growth mechanism, shape evolution and their application into Li-ion batteries, International Journal of Hydrogen Energy (2016), http://dx.doi.org/10.1016/j.ijhydene.2016.05.193

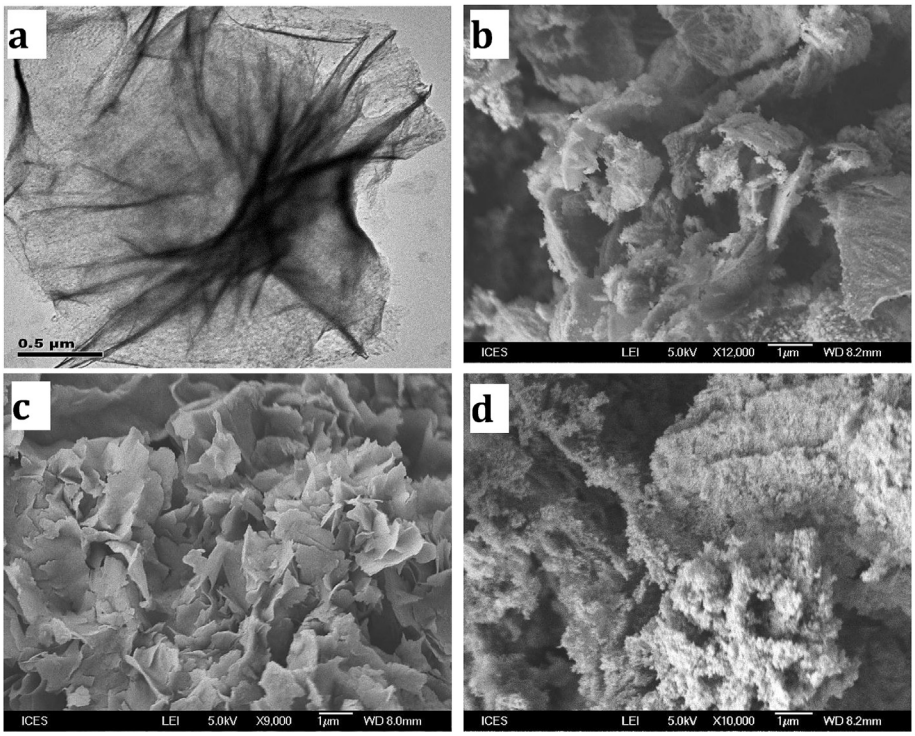

Fig. 5 – (a) TEM image of S1 after a reaction time of 2.5h; SEM images of (b) S2 (c) S3 and (d) S4.

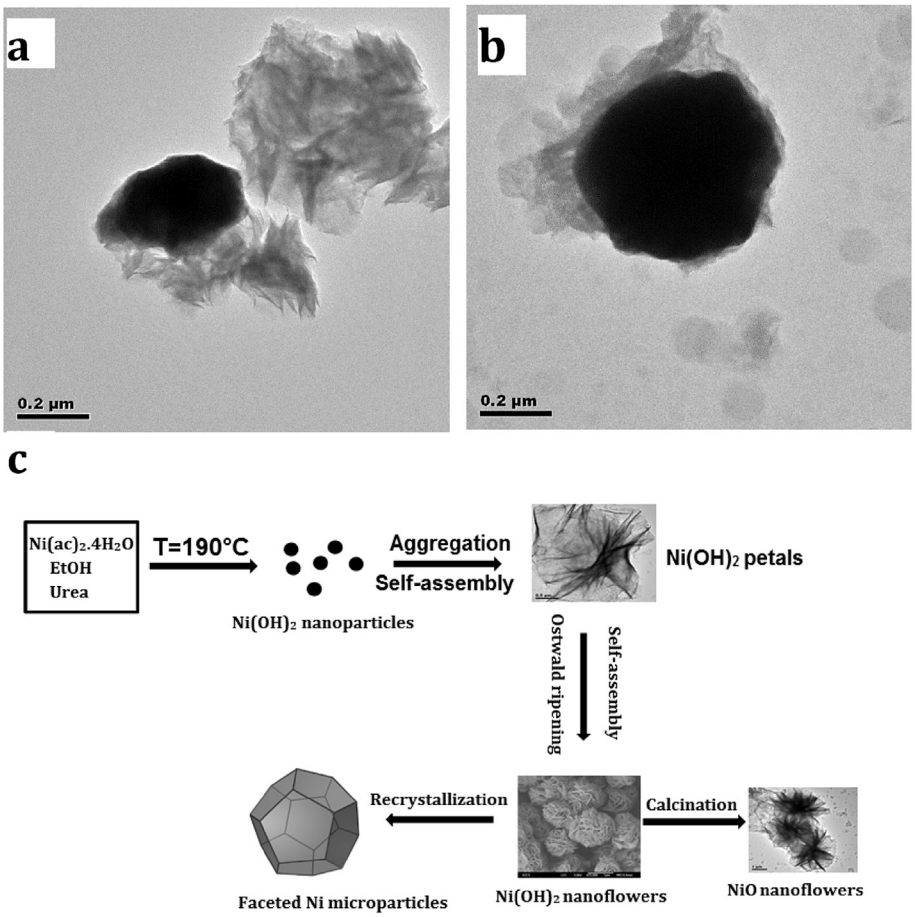

Fig. 6 – TEM images of S1 after (a) 4 h and (b) 4.5 h; (c)Schematic illustration of the formation process of NiO nanoflowers.

Please cite this article in press as: Mollamahale YB, et al., Simple fabrication of porous NiO nanoflowers: Growth mechanism, shape evolution and their application into Li-ion batteries, International Journal of Hydrogen Energy (2016), http://dx.doi.org/10.1016/j.ijhydene.2016.05.193

which a nanoflower is transforming to a faceted microparticle. The sheets of nanoflower are discrete which then undergo a packed self-assembly in microparticle creating a faceted structure. The faceted microparticle morphology is nearly completed after 4.5 h (S1-4.5h) in Fig. 6b suggesting that the actual complete reaction time is no longer than 5 h. According to the above experimental results, a proposed formation mechanism is illustrated in Fig. 6c.

Electrochemical performance of the NiO nanoflowers

The as-prepared NiO nanoflowers were used as anode materials for Lithium-ion batteries and their electrochemical responses were examined. Fig. 7a represents the cyclic voltammetric (CV) curves of NiO nanoflowers over a potential range from 0.01 V to 3 V at the 1st, 2nd and 3rd scanning cycles at a scan rate of 0.5 mV^{-1}. In the first cathodic scan a strong broad peak located at 0.232 V together with a shoulder at around 0.66 V are observed corresponding to the initial reduction of NiO to metallic Ni and the formation of amorphous Li_2O ($NiO + 2Li^+ + 2e^- = Ni + Li_2O$(5)) as well as surface electrolyte interface (SEI) which is a polymeric gel-like layer containing ethylene-oxide-based oligomers, LiF, Li_2CO_3, and lithium alkyl carbonate ($ROCO_2Li$), respectively [23,29,39]. This peak shifts to more positive potentials (0.89 V) in the second scan due to activation of the electrode and becomes smaller.

In the anodic sweep, two distinct oxidation peaks are found located at 1.58 V and 2.28 V which corresponds to dissolution of SEI and the reverse reaction in which metallic Ni is oxidized to NiO, respectively [40]. The decrease in the peak current and the integrated area of the anodic peak in the anodic scan is attributed to the capacity loss during the charging process [29]. After the activation in the first scan, the second and third cycles show similar potentials indicating the reversibility of the electrochemical cell becomes better after the second cycle and thus a stable electrochemical reaction between Li^+ and NiO has been set up. Fig. 7b compares the CV curves of the different prepared NiO nanostructures including NiO nanoflowers, and NiO microparticles (S1-8h and S1-24h) obtained after calcination at 400 °C for 1 h. The amount of currents in NiO nanoflowers are much higher, by far, suggesting that the NiO nanoflowers electrode is a strong electrode due to the large surface area and hence the most suitable material for lithium-ion batteries, here, as expected.

Fig. 8a shows the galvanostatic charge–discharge curves of NiO nanoflowers electrode as a function of specific capacity for the first two cycles at a constant current rate of 0.1 C in the potential range of 0.01 V–3 V. In the first discharge (Li^+ insertion), there is an initial drop in potential and then the curve shows a plateau at around 0.6 V corresponding to the reduction of NiO to Ni (reaction 5) which is extended to a capacity of about 1000 $mAhg^{-1}$. The sloping part in the end of the discharge curve between 0.6 and 0.01 V corresponds to the formation of the SEI layer [41]. The corresponding discharge capacity is 1936.9 $mAhg^{-1}$. The large specific surface area of NiO nanoflowers provides more contact area between NiO and electrolyte and offers more sites to accommodate Li^+, leading to high initial discharge capacity. Yet, this value is much higher than the theoretical capacity of 718 $mAhg^{-1}$ based on the reaction 9. The extra capacity is mainly due to the decomposition of non-aqueous electrolyte during the discharge process [29].

There are two slopes around 1.1 and 2.5 V in the first charge cycle and a reversible charge (Li^+ deinsertion) capacity of 1114 $mAhg^{-1}$ was obtained. As noted, the irreversible capacity loss is mainly due to the formation of SEI film [42].

The second discharge curve is different from the first one and the plateau is more slopped and shows a higher value (1.1 V) indicating that the Li^+ insertion would be easier due to the fast kinetic within the structure, as it is frequently reported [42,43]. The second discharge and charge capacities are 1286.8 and 956.2 $mAhg^{-1}$ which are yet relatively high. The second charge profile is very similar to the first one indicating stability of the electrode.

The lithium storage capacity of the NiO nanoflowers was evaluated through galvanostatic charge–discharge cycling at a current rate of 0.1 C. Fig. 8b depicts that the values of discharge capacities for the first 10 cycles are near to

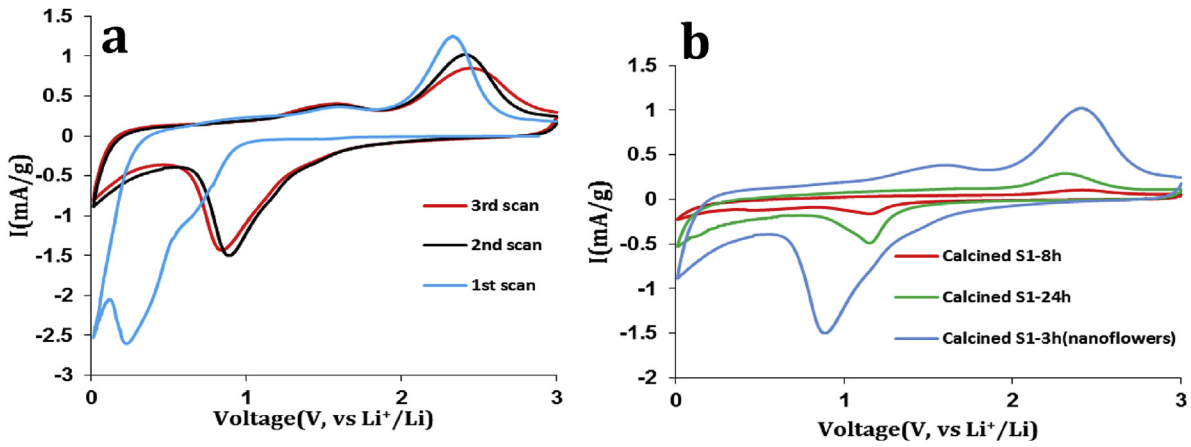

Fig. 7 – CV curves of (a) NiO nanoflowers electrode for the first three cycles (b) the prepared NiO nanostructures including different NiO microparticles (Red and green lines) and NiO nanoflowers (blue line) at the second cycle at a scan rate of 0.5 mV/s. (For interpretation of the references to colour in this figure legend, the reader is referred to the web version of this article.)

Please cite this article in press as: Mollamahale YB, et al., Simple fabrication of porous NiO nanoflowers: Growth mechanism, shape evolution and their application into Li-ion batteries, International Journal of Hydrogen Energy (2016), http://dx.doi.org/10.1016/j.ijhydene.2016.05.193

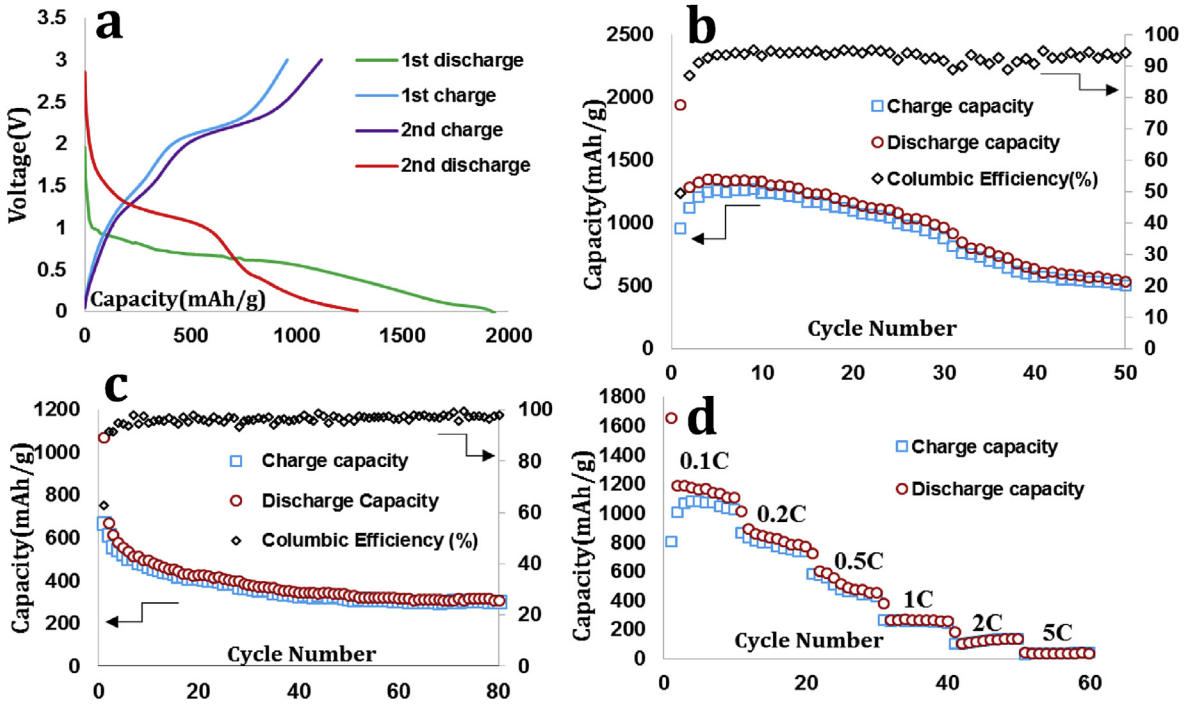

Fig. 8 – (a) Charge-discharge curves of NiO nanoflowers between 0.01 and 3.0 V at a current density of 0.1 C for the first two cycles (b) and (c) Specific capacity and columbic efficiency of NiO nanoflowers as a function of the cycle number at current rates of 0.1 C and 1 C, respectively, between 0.01 and 3.0 V and (d) rate capability of NiO nanoflowers at various current densities.

1330 mAh g^{-1} with excellent charge reversibility and a columbic efficiency of 94%. In the following cycles, the values however, gradually decrease to reach a plateau after 40 cycles and a discharge capacity of 551.8 mAh g^{-1} after 50 cycles with a high columbic efficiency of 94.1%. Fig. 8c demonstrates capacity values at a high current rate of 1 C for NiO nanoflowers which represents a good cyclability. The amount of capacity is maintained at 306.8 mAh g^{-1} with a very high columbic efficiency of 98% after 80 cycles which is quite good at such a high current density. Table 2 highlights the electrochemical properties of the prepared nanoflowers and similar NiO nanostructures fabricated by other researchers. In comparison with other structures like NiO nanotubes [27], Ni–NiO nanocomposites [42], 3D porous NiO [43], and flower-like NiO microspheres [44], the NiO nanoflowers electrode presents a good and stable discharge capacity.

The rate capability of NiO nanoflowers at different current rates from 0.1 C to 5 C between 0.01 and 3 V is represented in Fig. 8d. The charge–discharge capacity values decrease with an increase in current density which could be ascribed to lower Li^+ diffusion rate into NiO nanoflowers [42]. The NiO nanoflowers electrode shows a good performance at low

Table 2 – Summaries of the electrochemical properties of the NiO nanoflowers prepared in this work with other reported NiO nanostructures.

Sample	Current density (mA/g)	Potential range(V)	Initial capacity (mAh/g)	Capacity retention (mAh/g)	Reference
NiO nanotubes	25	0.01–3.0	610	200 after 200 cycles	[27]
NiO microspheres	50	0.01–3.0	1570	80 after 30 cycles	[37]
Hollow NiO microspheres	100	0.02–3.0	1100	560 after 50 cycles	[39]
NiO nanospheres	100	0.01–3.0	1200	518 after 60 cycles	[41]
NiO–Ni nanocomposite	286	0.02–3	503	420 after 100 cycles	[42]
Three-dimensional porous NiO	200	0.05–3.0	800	520 after 30 cycles	[43]
Flower-like NiO microspheres	50	0.01–3.0	1104	105 after 30 cycles	[44]
Urchin-like NiO microspheres	50	0.01–3.0	1295	134 after 50 cycles	[44]
Electrospun NiO nanofibers	100	0.005–3.0	1280	583 after 100 cycles	[45]
Porous NiO nanoparticles	15	0.01–3.0	900	380 after 100 cycles	[46]
Hierarchical NiO nano/microspheres	100	0.01–3.0	1165	720 after 100 cycles	[47]
Hierarchical NiO microsphere	700	0.005–3.0	1452	598 after 100 cycles	[48]
Hollow NiO nanotubes	200	0.01–3.0	1072	600 after 100 cycles	[49]
NiO nanoflowers	100	0.01–3.0	1936.9	552 after 50 cycles	This work

Please cite this article in press as: Mollamahale YB, et al., Simple fabrication of porous NiO nanoflowers: Growth mechanism, shape evolution and their application into Li-ion batteries, International Journal of Hydrogen Energy (2016), http://dx.doi.org/10.1016/j.ijhydene.2016.05.193

current rates which could be referred to smaller charge resistance and large surface area [29]. However, at high current rates such as 5 C, the specific storage capacity dramatically decreases. The decrement of storage capacity could be referred to the structural damage due to the large volume expansion/constriction which also follows by continues destroy and formation of SEI and continuous consumption of the electrolyte [37]. Yet, it is interesting that when current rate was switched again to 0.1 C after 60 cycles, a specific discharge capacity of 933.7 $mAhg^{-1}$ was maintained which shows the electrode could still perform good.

Conclusion

A simple solvothermal method was developed to fabricate NiO nanoflowers via α-$Ni(OH)_2$. It was found that ethanol, urea and nickel source had key roles on developing the nanoflowers morphology. The fabricated NiO nanoflowers showed promising results as anode material for lithium-ion batteries which could be referred to their high surface area and short diffusion length. Under high current rate of 1 C, the electrode demonstrated an initial discharge capacity of 671.2 $mAhg^{-1}$ and a stable capacity of 306.8 $mAhg^{-1}$ even after 80 cycles with a high columbic efficiency of 98%. However, further improvement in electrochemical properties and cyclic stability is still needed.

Acknowledgments

Authors are thankful to Collaborative Innovation Center of Renewal Energy Materials, Guangxi University, Nanning, China and Institute of Chemical and Engineering Sciences, A*STAR (Agency for Science, Technology and Research) for supporting the project.

REFERENCES

[1] Gu L, Xie W, Bai S, Liu B, Xue S, Li Q, et al. Facile fabrication of binder-free NiO electrodes with high rate capacity for lithium-ion batteries. Appl Surf Sci 2016;368:298–302.
[2] Mai YJ, Tu JP, Xia XH, Gu CD, Wang XL. Co-doped NiO nanoflake arrays toward superior anode materials for lithium ion batteries. J Power Sources 2011;196:6388–93.
[3] Li Y, Tan B, Wu Y. Mesoporous Co_3O_4 nanowire arrays for lithium ion batteries with high capacity and rate capability. Nano Lett 2008;8:265–70.
[4] Kawamori M, Asai T, Shirai Y, Yagi S, Oishi M, Ichitsubo T, et al. Three-dimensional nanoelectrode by metal nanowire nonwoven clothes. Nano Lett 2014;14:1932–7.
[5] Wu H, Xu M, Wang Y, Zheng G. Branched Co_3O_4/Fe_2O_3 nanowires as high capacity lithium-ion battery anodes. Nano Res 2013;6:167–73.
[6] Liu B, Zhang J, Wang X, Chen G, Chen D, Zhou C, et al. Hierarchical three-dimensional $ZnCo_2O_4$ nanowire arrays/carbon cloth anodes for a novel class of high-performance flexible lithium-ion batteries. Nano Lett 2012;12:3005–11.
[7] Cheng F, Tao Z, Liang J, Chen J. Template-directed materials for rechargeable lithium-ion batteries. Chem Mater 2008;20:667–81.
[8] Li WY, Xu LN, Chen J. Co_3O_4 nanomaterials in lithium-ion batteries and gas sensors. Adv Funct Mater 2005;15:851–7.
[9] He BL, Dong B, Li HL. Preparation and electrochemical properties of Ag-modified TiO_2 nanotube anode material for lithium–ion battery. Electrochem Commun 2007;9:425–30.
[10] Li X, Li D, Qiao L, Wang X, Sun X, Wang P, et al. Interconnected porous MnO nanoflakes for high-performance lithium ion battery anodes. J Mater Chem 2012;22:9189–94.
[11] Chun L, Wu X, Lou X, Zhang Y. Hematite nanoflakes as anode electrode materials for rechargeable lithium-ion batteries. Electrochim Acta 2010;55:3089–92.
[12] Liu J, Jiang J, Bosman M, Fan HJ. Three-dimensional tubular arrays of MnO2–NiO nanoflakes with high areal pseudocapacitance. J Mater Chem 2012;22:2419–26.
[13] Zeng S, Tang K, Li T, Liang Z, Wang D, Wang Y, et al. Facile route for the fabrication of porous hematite nanoflowers: Its synthesis, growth mechanism, application in the lithium ion battery, and magnetic and photocatalytic properties. J Phys Chem C 2008;112:4836–43.
[14] Lin YS, Tsai MC, Duh JG. Self-assembled synthesis of nanoflower-like $Li_4Ti_5O_{12}$ for ultrahigh rate lithium-ion batteries. J Power Sources 2012;214:314–8.
[15] Vaughn DD, Hentz OD, Chen S, Wangand D, Schaak RE. Formation of SnS nanoflowers for lithium ion batteries. Chem Commun 2012;48:5608–10.
[16] Xiang JY, Tu JP, Yuan YF, Wang XL, Huang XH, Zeng ZY. Electrochemical investigation on nanoflower-like CuO/Ni composite film as anode for lithium ion batteries. Electrochim Acta 2009;54:1160–5.
[17] Wu HB, Chen JS, Hng HH, Lou XW. Nanostructured metal oxide-based materials as advanced anodes for lithium-ion batteries. Nanoscale 2012;4:2526–42.
[18] Meduri P, Pendyala C, Kumar V, Sumanasekera GU, Sunkara MK. Hybrid tin oxide nanowires as stable and high capacity anodes for Li-ion batteries. Nano Lett 2009;9:612–6.
[19] Xiao J, Yang S. Sequential crystallization of sea urchin-like bimetallic (Ni, Co) carbonate hydroxide and its morphology conserved conversion to porous $NiCo_2O_4$ spinel for pseudocapacitors. RSC Adv 2011;1:588–95.
[20] Poizot P, Laruelle S, Grugeon S, Dupont L, Tarascon JM. Nano-sized transition-metal oxides as negative-electrode materials for lithium-ion batteries. Nature 2000;407:496–9.
[21] Zhao B, Ke XK, Bao JH, Wang CL, Dong L, Chen YW, et al. Synthesis of flower-like NiO and effects of morphology on its catalytic properties. J Phys Chem C 2009;113:14440–7.
[22] Zhang X, Shi W, Zhu J, Zhao W, Ma J, Mhaisalkar S, et al. Synthesis of porous NiO nanocrystals with controllable surface area and their application as supercapacitor electrodes. Nano Res 2010;3:643–52.
[23] Hwang SG, Kim GOK, Yun SR, Ryu KS. NiO nanoparticles with plate structure grown on graphene as fast charge–discharge anode material for lithium ion batteries. Electrochim Acta 2012;78:406–11.
[24] Su D, Kim HS, Kim WS, Wang G. Mesoporous nickel oxide nanowires: hydrothermal synthesis, characterisation and applications for lithium-Ion batteries and supercapacitors with superior performance. Chem Eur J 2012;18:8224–9.
[25] Wang X, Li L, Zhang Y, Wang S, Zhang Z, Fei L, et al. High-yield synthesis of NiO nanoplatelets and their excellent electrochemical performance. Cryst Growth Des 2006;6:2163–5.
[26] Varghese B, Reddy MV, Yanwu Z, Lit CS, Hoong TC, Subba Rao GV, et al. Fabrication of NiO nanowall electrodes for high

Please cite this article in press as: Mollamahale YB, et al., Simple fabrication of porous NiO nanoflowers: Growth mechanism, shape evolution and their application into Li-ion batteries, International Journal of Hydrogen Energy (2016), http://dx.doi.org/10.1016/j.ijhydene.2016.05.193

performance lithium ion battery. Chem Mater 2008;20:3360–7.
[27] Needham SA, Wang GX, Liu HK. Synthesis of NiO nanotubes for use as negative electrodes in lithium ion batteries. J Power Sources 2006;159:254–7.
[28] Zhu LP, Liao GH, Yang Y, Xiao HM, Wang JF, Fu SY. Self-assembled 3D flower-like hierarchical β-$Ni(OH)_2$ hollow architectures and their in situ thermal conversion to NiO. Nanoscale Res Lett 2009;4:550–7.
[29] Li Q, Chen Y, Yang T, Lei D, Zhang G, Mei L, et al. Preparation of 3D flower-like NiO hierarchical architectures and their electrochemical properties in lithium-ion batteries. Electrochim Acta 2013;90:80–9.
[30] Cao F, Zhang F, Deng R, Liu D, Hu W, Song S, et al. Surfactant-free preparation of NiO nanoflowers and their lithium storage properties. Cryst Eng Commun 2011;13:4903–8.
[31] Meher SK, Justin P, Rao GR. Microwave-mediated synthesis for improved morphology and pseudocapacitance performance of nickel oxide. ACS Appl Mater Interfaces 2011;3:2063–73.
[32] Zhu Z, Wei N, Liu H, He Z. Microwave-assisted hydrothermal synthesis of $Ni(OH)_2$ architectures and their in situ thermal convention to NiO. Adv Powder Technol 2011;22:422–6.
[33] Ran S, Zhu Y, Huang H, Liang B, Liu B, Xu J, et al. Phase-controlled synthesis of 3D flower-like $Ni(OH)_2$ architectures and their applications in water treatment. Cryst Eng Commun 2012;14:3063–8.
[34] Yang ZX, Zhong W, Au C, Wang JY, Du YW. An environment-benign solvothermal method for the synthesis of flower-like hierarchical nickel and zinc compounds and their transformation to nanoporous NiO and ZnO. Cryst Eng Commun 2011;13:1831–7.
[35] Ma J, Yang J, Jiao L, Mao Y, Wang T, Duan X, et al. NiO nanomaterials: controlled fabrication, formation mechanism and the application in lithium-ion battery. Cryst Eng Commun 2012;14:453–9.
[36] Wei XW, Zhou XM, Wu KL, Chen Y. 3-D flower-like NiCo alloy nano/microstructures grown by a surfactant-assisted solvothermal process. Cryst Eng Commun 2011;13:1328–32.
[37] Liu L, Li Y, Yuan S, Ge M, Ren M, Sun C, et al. Nanosheet-based NiO microspheres: controlled solvothermal synthesis and lithium storage performances. J Phys Chem C 2010;114:251–5.
[38] Yang LX, Zhu YJ, Tong H, Liang ZH, Li L, Zhang L. Hydrothermal synthesis of nickel hydroxide nanostructures in mixed solvents of water and alcohol. J Solid State Chem 2007;180:2095–101.
[39] Huang XH, Tu JP, Zhang CQ, Zhou F. Hollow microspheres of NiO as anode materials for lithium-ion batteries. Electrochim Acta 2010;55:8981–5.
[40] Ni S, Li T, Yang X. Fabrication of NiO nanoflakes and its application in lithium ion battery. Mater Chem Phys 2012;132:1108–11.
[41] Zhang G, Chen Y, Qu B, Hu L, Mei L, Lei D, et al. Synthesis of mesoporous NiO nanospheres as anode materials for lithium ion batteries. Electrochim Acta 2012;80:140–7.
[42] Li X, Dhanabalan A, Wang C. Enhanced electrochemical performance of porous NiO–Ni nanocomposite anode for lithium ion batteries. J Power Sources 2011;196:9625–30.
[43] Wang C, Wang D, Wang Q, Chen H. Fabrication and lithium storage performance of three-dimensional porous NiO as anode for lithium-ion battery. J Power Sources 2010;195:7432–7.
[44] Pan JH, Huang Q, Koh ZY, Jin C, Neo D, Wang XZ, et al. Scalable synthesis of urchin and flower-like hierarchical NiO microspheres and their electrochemical property for lithium storage. ACS Appl Mater Interfaces 2013;5:6292–9.
[45] Aravindan V, Kumar PS, Sundaramurthy J, Ling WC, Ramakrishna S, Madhavi S. Electrospun NiO nanofibers as high performance anode material for Li-ion batteries. J Power Sources 2013;227:284–90.
[46] Zhang F, Jiang D, Zhang X. Porous NiO materials prepared by solid-state thermolysis of a Ni-MOF crystal for lithium-ion battery anode. Nano Struct Nano Objects 2016;5:1–6.
[47] Wang Q, Xu YF, Xu GL, Su H, Shen SY, Tu TT, et al. Synthesis of hierarchical NiO microsphere with waxberry-like structure and its enhanced lithium storage performance. J Alloys Compd 2015;648:59–66.
[48] Lv P, Zhao H, Zeng Z, Gao C, Liu X, Zhang T. Self-assembled three-dimensional hierarchical NiO nano/microspheres as high performance anode material for lithium ion batteries. App Surf Sci 2015;329:301–5.
[49] Liu L, Guo Y, Wang Y, Yang X, Wang S, Guo H. Hollow NiO nanotubes synthesized by bio-templates as the high performance anode materials of lithium-ion batteries. Electrochim Acta 2013;114:42–7.

Please cite this article in press as: Mollamahale YB, et al., Simple fabrication of porous NiO nanoflowers: Growth mechanism, shape evolution and their application into Li-ion batteries, International Journal of Hydrogen Energy (2016), http://dx.doi.org/10.1016/j.ijhydene.2016.05.193